AMSI VACATIONRESEARCH SCHOLARSHIPS 2022–23

SET YOUR SIGHTS ON RESEARCH THIS SUMMER

# Investigating spontaneous symmetry breaking of spatial Kerr solitons in fractional spatial dimensions using Fourier spectral methods

Brenton Horne

Supervised by Associate Professor Dmitry Strunin

University of Southern Queensland

AMSI AUSTRALIAN MATHEMATICAL SCIENCES INSTITUTE

**Abstract**

The aim of this study is to use coupled nonlinear fractional Schrödinger equations (NFSE) to investigate spontaneous symmetry breaking of Kerr solitons. This was achieved using numerical integration in MATLAB R2022b. Fast Fourier transforms were used to approximate spatial derivatives using spatial grid point values and a fourth-order Runge-Kutta scheme was used to integrate the solution on time. The model generated showed the conditions under which spontaneous symmetry breaking of Kerr solitons occurred. It allowed for collisions of humps and stable solitons to be simulated and the behaviour of the post-collision solitons to be examined. It also allowed for collisions of asymmetric solitons to be simulated and their post-collision behaviour to be examined. Additionally, the collision of tall and short solitons was also simulated and the post-collision behaviour examined.

# Introduction

Spontaneous symmetry breaking (SSB) is the spontaneous transformation of symmetric and antisymmetric states into asymmetric states (Li et al., 2020). It is a ubiquitous phenomenon and hence its study is immensely useful (Li et al., 2020). In this study, SSB of Kerr solitons were studied using coupled nonlinear fractional Schrödinger equations.

The dimensionless coupled nonlinear fractional Schrödinger equations used in this project were (Driben and Malomed, 2011):

$$i\frac{\partial u_1}{\partial t} - \frac{1}{2}\left(-\frac{\partial^2}{\partial x^2}\right)^{\alpha/2} u_1 + |u_1|^2 u_1 + u_2 = 0, \tag{1}$$

$$i\frac{\partial u_2}{\partial t} - \frac{1}{2}\left(-\frac{\partial^2}{\partial x^2}\right)^{\alpha/2} u_2 + |u_2|^2 u_2 + u_1 = 0. \tag{2}$$

Equations (1) and (2) are a particular case of Equation (1) in Driben and Malomed (2011) when $\gamma = \Gamma = 0$ and $\kappa = 1$. Here $u_1(x,t)$ and $u_2(x,t)$ are scaled versions of the wave function; their magnitude is proportional to the probability density function for the particle they describe. In this report, Equations (1) and (2) were solved using a combination of fast Fourier transforms for approximating spatial derivatives and the Runge-Kutta fourth-order method for integrating the solution on time. Several different initial conditions (including those corresponding to stable solitons by themselves, stable solitons on collision courses with humps, asymmetric solitons on collision courses with each other and tall and short solitons on collision courses with each other) were tried with the results visualised using waterfall plots in order to study SSB in a few different circumstances.

## Statement of authorship

Dmitry Strunin supervised this project, provided Equations (1) and (2) and the $\xi = x - ct$ transformation (and mentioned how this transformation would affect the partial derivatives in Equations (1) and (2)), suggested possible experiments that should be conducted, provided information about how the results should be interpreted, proofed this report and provided the data files (for the initial conditions) used for the simulations described in this report. He also provided the code to import these data files into MATLAB. The code used to perform the analysis was based on Program 2 found on page 329 of Yang (2010) although adapted by Brenton Horne to meet the requirements of this project. This report was written by Brenton Horne.

## Method

Equations (1) and (2) were transformed to $(\xi, t)$ coordinates using $\xi = x - ct$, where $c$ is the constant propagation velocity of the soliton. The partial derivatives became:

$$\frac{\partial}{\partial t} \text{ (old formulation)} = \frac{\partial}{\partial t} \text{ (new formulation)} + \frac{\partial \xi}{\partial t}\frac{\partial}{\partial \xi}, \tag{3}$$

$$\frac{\partial}{\partial x} = \frac{\partial}{\partial \xi}. \tag{4}$$

Here $\dfrac{\partial \xi}{\partial t} = -c$ and hence $\dfrac{\partial}{\partial t}$ (old formulation) is:

$$\frac{\partial}{\partial t} \text{ (old formulation)} = \frac{\partial}{\partial t} \text{ (new formulation)} - c\frac{\partial}{\partial \xi}. \tag{5}$$

Consequently, Equations (1) and (2) become:

$$i\frac{\partial u_1}{\partial t} - ic\frac{\partial u_1}{\partial \xi} - \frac{1}{2}\left(-\frac{\partial^2}{\partial \xi^2}\right)^{\alpha/2} u_1 + |u_1|^2 u_1 + u_2 = 0, \tag{6}$$

$$i\frac{\partial u_2}{\partial t} - ic\frac{\partial u_1}{\partial \xi} - \frac{1}{2}\left(-\frac{\partial^2}{\partial \xi^2}\right)^{\alpha/2} u_2 + |u_2|^2 u_2 + u_1 = 0. \tag{7}$$

The Runge-Kutta fourth-order (RK4) integration scheme is most easily applicable when a system of partial differential equations is written in the form:

$$\frac{\partial u_1}{\partial t} = F_1(\xi, t, u_1, u_2), \tag{8}$$

$$\frac{\partial u_2}{\partial t} = F_2(\xi, t, u_1, u_2). \tag{9}$$

Spatial partial derivatives of $u_1$ and $u_2$ can be included in $F_1$ and $F_2$ so long as they can be efficiently approximated from $u_1$ and $u_2$ (such as using a fast Fourier transform). To rewrite Equations (6) and (7) in the form of Equations (8) and (9) first divide Equations (6) and (7) by $i$ and then move every term that does not involve partial derivatives with respect to time to the right-hand side:

$$\frac{\partial u_1}{\partial t} = c\frac{\partial u_1}{\partial \xi} - \frac{i}{2}\left(-\frac{\partial^2}{\partial \xi^2}\right)^{\alpha/2} u_1 + i|u_1|^2 u_1 + iu_2, \tag{10}$$

$$\frac{\partial u_2}{\partial t} = c\frac{\partial u_2}{\partial \xi} - \frac{i}{2}, \left(-\frac{\partial^2}{\partial \xi^2}\right)^{\alpha/2} u_2 + i|u_2|^2 u_2 + iu_1. \tag{11}$$

Spatial partial derivatives in Equations (10) and (11) were approximated using a fast Fourier transform (FFT), namely as:

$$\frac{\partial \mathbf{u}_1}{\partial t} = c\,\mathrm{ifft}(ik\,\mathrm{fft}(\mathbf{u}_1)) - \frac{i}{2}\mathrm{ifft}(|k|^\alpha \mathrm{fft}(\mathbf{u}_1)) + i|\mathbf{u}_1|^2\mathbf{u}_1 + i\mathbf{u}_2, \tag{12}$$

$$\frac{\partial \mathbf{u}_2}{\partial t} = c\,\mathrm{ifft}(ik\,\mathrm{fft}(\mathbf{u}_2)) - \frac{i}{2}\mathrm{ifft}(|k|^\alpha \mathrm{fft}(\mathbf{u}_2)) + i|\mathbf{u}_2|^2\mathbf{u}_2 + i\mathbf{u}_1. \tag{13}$$

Where fft(.) is a FFT, ifft(.) is an inverse FFT, $k$ is the wavenumber and $\mathbf{u}_1$ and $\mathbf{u}_2$ are vectors comprised of functions (of time) representing the value of $u_1$ and $u_2$, respectively, at each grid point. Let the right-hand side of Equation (12) be called RHS($c$, $k$, $\alpha$, $u_1$, $u_2$). Consequently, the right-hand side of Equation (13) can be written as RHS($c$, $k$, $\alpha$, $u_2$, $u_1$) due to the symmetry of the coupled nonlinear fractional NFSEs. Let $\mathbf{u}_{1,j}$ denote a vector of spatial $u_1$ values for the $j$th time point in the simulation, $\mathbf{u}_{2,j}$ denote a vector of spatial $u_2$ values for the $j$th time point in the simulation and $dt$ denote the increment between time steps (which is assumed to be constant). Therefore the RK4 approximation to Equations (12) and (13) is:

$$\mathbf{l}_1 = dt \times \text{RHS}(c, k, \alpha, \mathbf{u}_{1,j}, \mathbf{u}_{2,j}), \tag{14}$$

$$\mathbf{m}_1 = dt \times \text{RHS}(c, k, \alpha, \mathbf{u}_{2,j}, \mathbf{u}_{1,j}), \tag{15}$$

$$\mathbf{l}_2 = dt \times \text{RHS}\left(c, k, \alpha, \mathbf{u}_{1,j} + \frac{1}{2}\mathbf{l}_1, \mathbf{u}_{2,j} + \frac{1}{2}\mathbf{m}_1\right), \tag{16}$$

$$\mathbf{m}_2 = dt \times \text{RHS}\left(c, k, \alpha, \mathbf{u}_{2,j} + \frac{1}{2}\mathbf{m}_1, \mathbf{u}_{1,j} + \frac{1}{2}\mathbf{l}_1\right), \tag{17}$$

$$\mathbf{l}_3 = dt \times \text{RHS}\left(c, k, \alpha, \mathbf{u}_{1,j} + \frac{1}{2}\mathbf{l}_2, \mathbf{u}_{2,j} + \frac{1}{2}\mathbf{m}_2\right), \tag{18}$$

$$\mathbf{m}_3 = dt \times \text{RHS}\left(c, k, \alpha, \mathbf{u}_{2,j} + \frac{1}{2}\mathbf{m}_2, \mathbf{u}_{1,j} + \frac{1}{2}\mathbf{l}_2\right), \tag{19}$$

$$\mathbf{l}_4 = dt \times \text{RHS}\left(c, k, \alpha, \mathbf{u}_{1,j} + \mathbf{l}_3, \mathbf{u}_{2,j} + \mathbf{m}_3\right), \tag{20}$$

$$\mathbf{m}_4 = dt \times \text{RHS}\left(c, k, \alpha, \mathbf{u}_{2,j} + \mathbf{m}_3, \mathbf{u}_{1,j} + \mathbf{l}_3\right), \tag{21}$$

$$\mathbf{u}_{1,j+1} = \mathbf{u}_{1,j} + \frac{1}{6}\left(\mathbf{l}_1 + 2\mathbf{l}_2 + 2\mathbf{l}_3 + \mathbf{l}_4\right), \tag{22}$$

$$\mathbf{u}_{2,j+1} = \mathbf{u}_{2,j} + \frac{1}{6}\left(\mathbf{m}_1 + 2\mathbf{m}_2 + 2\mathbf{m}_3 + \mathbf{m}_4\right). \tag{23}$$

Equations (14)–(23) were used in this study to approximate $u_1$ and $u_2$. The time step, $dt$, was usually set to 0.001, except when simulations had to be performed over longer periods of time (that is, when $t_{\max} > 40$, where $t_{\max}$ is the time length of the simulation) or when multiple simulations had to be performed quickly (like when the $A\text{sech}(B\xi)$ initial condition was tested for multiple different $A$ and $B$ values). A variable called $L$ was defined as equalling 30 and $\xi$ ranged from $-\frac{L}{2}$ to $\frac{L}{2} - d\xi$ where $d\xi$ is the size of the increments in $\xi$ (which is $L$ divided by the number of spatial steps, which was called $N$ and was set to 600 for each simulation). $t$ ranged from 0 to $t_{\max}$.

Several different initial conditions for $u_1$ and $u_2$ were tried; the specifics are mentioned later. They were then added to the first column of matrices called u1data and u2data, respectively. These matrices were of size $N \times (n_{\max} + 1)$, where $n_{\max}$ is the number of time steps used in the simulation (an additional column is required to store the initial conditions). A row vector was also created of size $n_{\max} + 1$ that was called tdata and its purpose was to store values of time corresponding to the values of u1 and u2 in u1data and u2data, respectively. The first entry of tdata was zero (corresponding to $t = 0$ which is the time for the initial conditions). The different columns of the u1data and u2data matrices corresponded to different time points in the simulation and the different rows to different $\xi$ values. Then over a loop Equations (14)–(23) were used to approximate $\mathbf{u}_{1,j}$ and $\mathbf{u}_{2,j}$ for each value of $j$ in the simulation. These vectors were stored in the appropriate column of u1data and u2data. Although due to the limitations in the waterfall graph (namely that it can only show so many time steps in a single graph) and to maximise how quickly the simulation ran only a set number of equally-spaced (in time) $\mathbf{u}_{1,j}$ and $\mathbf{u}_{2,j}$ vector pairs were added to these matrices (and only the time values corresponding to these pairs were added to the tdata vector).

Waterfall plots (with $\xi$ on the $x$-axis, $t$ on the $y$-axis and $|u|$ on the $z$-axis) for the absolute values of both $u_1$ and $u_2$ were generated with a black colour map, axes appropriately labelled (font size chosen for the labels was 15 pt) and axis limits set appropriately (namely to $-\dfrac{L}{2}$ to $\dfrac{L}{2}$ for the $x$-axis, 0 to $t_{\max}$ for the $y$-axis and 0 to 2 for the $z$-axis). The initial azimuth angle for the camera was set to $10^\circ$ and the initial elevation angle for the camera was set to $60^\circ$.

Using this script the evolution of soliton pairs with various different parameter values was examined.

Initially, the initial conditions of $u_1(\xi, t = 0) = A\text{sech}(B\xi)$ and $u_2(\xi, t = 0) = A\text{sech}(B\xi)$ were tried with $A$ and $B$ varied between (and including) 0.5 and 10 in increments of 0.5 with $\alpha = 1.6$ and $c = 0.4$. The goal of this simulation was to identify $A$ and $B$ values for which the solitons were stable.

Data files containing stable solitons were then used to provide the initial condition for the simulation, with $\alpha = 1.6$ and $c = 0.4$. The simulation was also conducted with $c = 0$.

The aforementioned stable soliton of $u_1$ was then moved to the left of the centre of the graph ($x = 0$) and a hump was added to the right of the centre of the graph for the initial condition. The solitons were moved to the left by deleting some of the initial condition data that pertained to negative $\xi$ values and extrapolating the function to the right by multiplying its right-most value (corresponding to highest $\xi$ value) by a decreasing exponential function of $\xi$. Specifically the MATLAB code:

```
left_shift = 2;
u1 = [u1_orig(left_shift*N/L+1:end);
u1_orig(end)*exp(-dxi*(1:left_shift*N/L)')];
```

where u1_orig contained the stable soliton imported from the data file and left_shift is how far to the left (of $\xi = 0$) the soliton was shifted, was used.

The humps were of the form

$$h_1(\xi, t=0) = b_1 \exp\left[-\frac{(\xi - \xi_0)^2}{c_1^2}\right], \tag{24}$$

$$h_2(\xi, t=0) = b_2 \exp\left[-\frac{(\xi - \xi_0)^2}{c_2^2}\right]. \tag{25}$$

Where $b_1$, $b_2$, $\xi_0$, $c_1$ and $c_2$ are constants. This was done for the purpose of simulating a collision between the solitons and the humps. For these simulations $c$ was set to 0.4.

Another simulation was conducted using asymmetric soliton pairs that were imported from data files. The goal was to observe a collision and observe the post-collision behaviour of the solitons, specifically to determine whether it was periodic or oscillatory.

Additionally, an initial condition wherein for $u_1$ there was a tall soliton on a collision course with a short soliton (with the tall soliton on the left-hand side of the graph, that is centred on negative $\xi$ values, and the short soliton centred on the right-hand side of the graph). $u_2$ had a similar initial condition, except with the locations of the tall and short solitons reversed (tall on the right, short on the left). This simulation was run with two different wave speeds (that is, $c$ values) namely $c = 0.5$ and $c = 0.8$. The initial conditions were also perturbed by adding sine waves to both $u_1$ and $u_2$ (of the form $a \sin \xi$, where $a$ is a specified amplitude).

# Results and discussion

The $A\text{sech}(B\xi)$ initial conditions lead to solitons that move to the left (negative $\xi$ direction) before starting again at the far-right (highest $\xi$ values) of the graph when $A$ and $B$ were the same and equal to 0.5 or 1. These solitons become slightly flatter and wider with time, although as this effect is reduced by reducing $dt$ it is possible this is due to numerical error. Other $A$ and $B$ values yielded very unstable waves that quickly degenerated into random noise. $A = 9$ and $B \leq 6.5$, and $A \geq 9.5$ (regardless of $B$) lead to $u_1$ and $u_2$ becoming undefined immediately after $t = 0$.

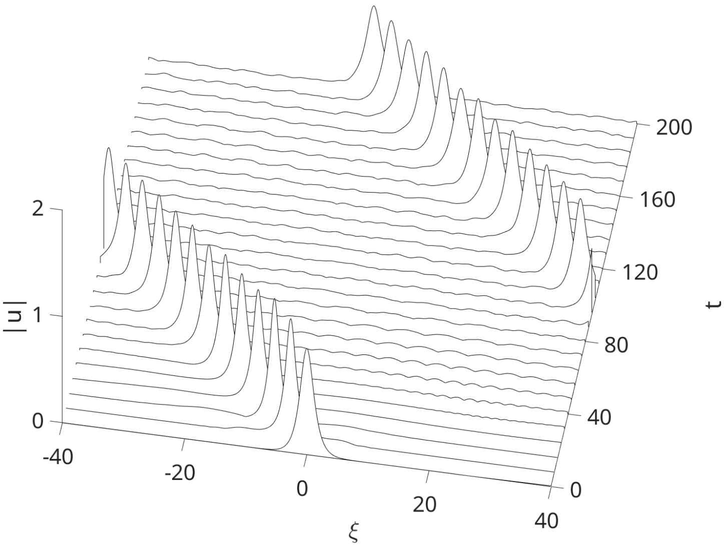

Figure 1: Time evolution of $u_1$ when $A = 1$ and $B = 1$. The $u_2$ graph looks more or less identical with the same initial condition. $dt = 0.006$ and $t_{\max} = 100$ for this simulation.

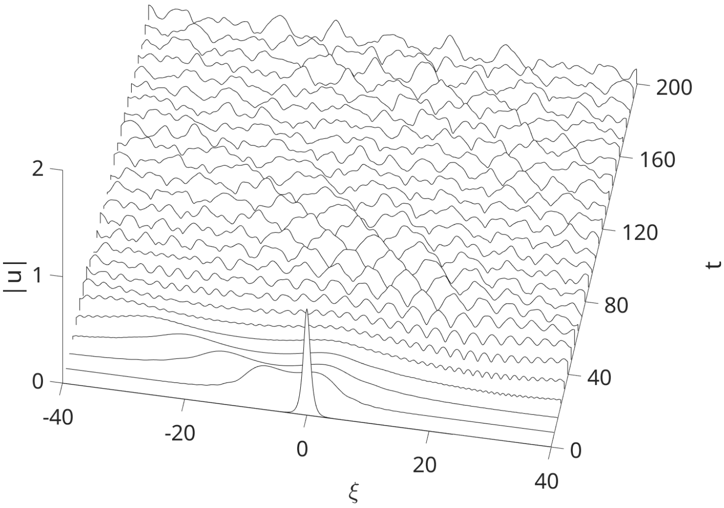

Figure 2: Time evolution of $u_1$ when $A = 1$ and $B = 2$. The $u_2$ graph looks more or less identical with the same initial condition. $dt = 0.006$ and $t_{\max} = 100$ for this simulation.

When the stable solitons were imported and simulated the solitons remained stable, although they moved to the right (towards higher $\xi$ values) when $c = 0$.

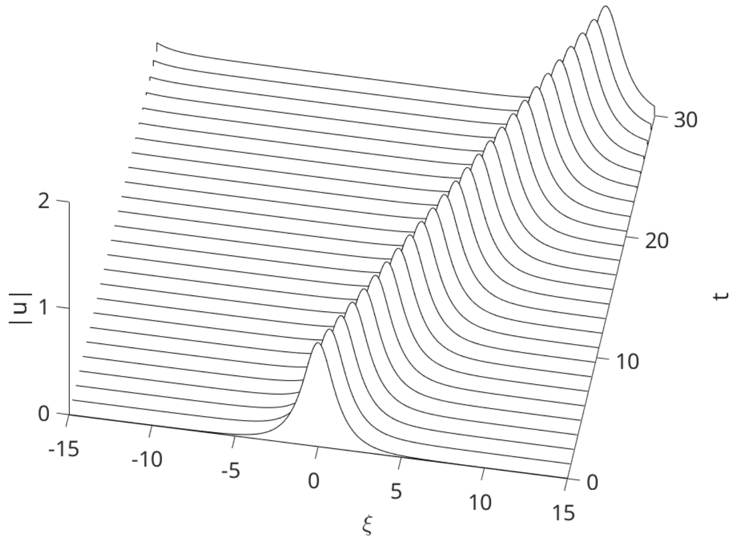

Figure 3: Stable soliton evolution over time when $\alpha = 1.6$ and $c = 0$. $dt = 0.001$ and $t_{\max} = 30$ for this simulation. This graph is for $u_1$ but $u_2$'s graph looks the same.

When the stable solitons were moved to the left (negative $\xi$ direction) and humps were added to the right of the centre of the graph (corresponding to $\xi_0 > 0$), the expected collisions occurred. The new soliton formed by the collision was not as stable as the original and seemed to oscillate.

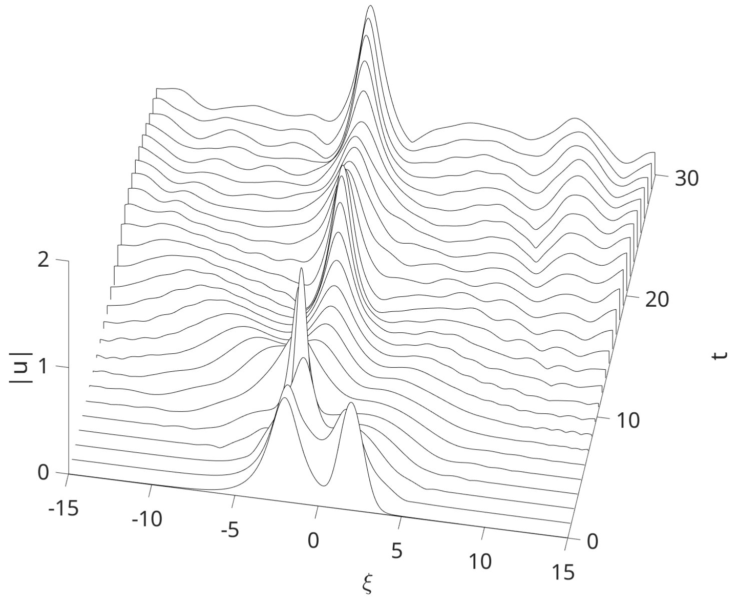

Figure 4: Stable soliton and hump, both centred 2 units from $\xi = 0$, colliding. All other hump parameters are set to 1. Plot shown is of $u_1$; $u_2$ has a similar plot.

When asymmetric soliton pairs were collided $u_2$ solitons usually did not survive the collision, whilst $u_1$ solitons continued with roughly the same height as the original solitons (although their height oscillated slightly).

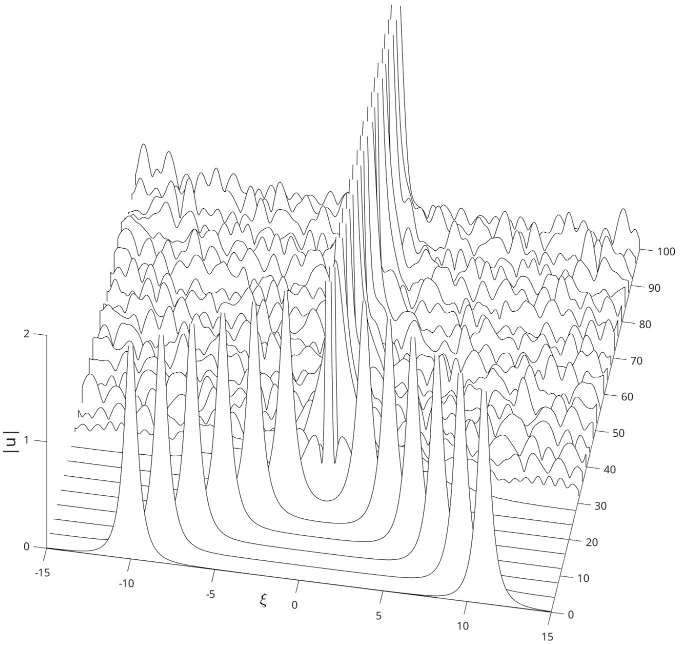

Figure 5: Plot of $u_1$ after asymmetric soliton collision. $c = 0$ and $dt = 0.003$ in this collision ($t_{\max} = 100$).

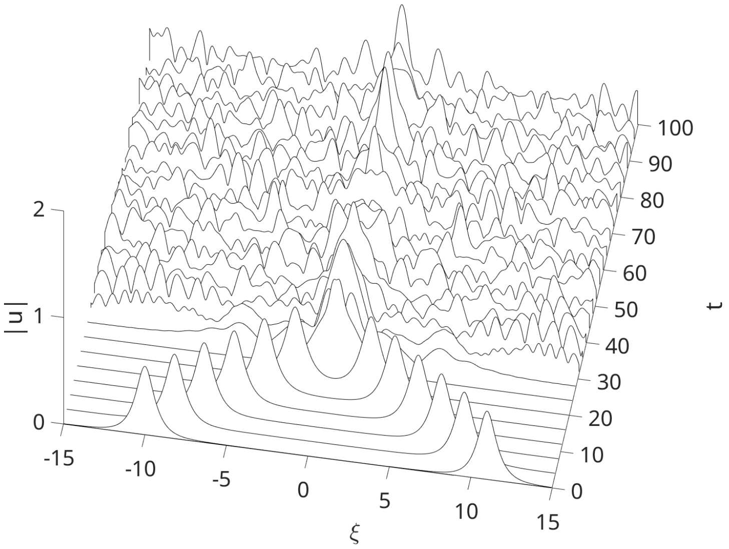

Figure 6: Plot of $u_2$ after asymmetric soliton collision. $c = 0$ and $dt = 0.003$ in this collision ($t_{\max} = 100$).

When tall and short solitons were collided without any perturbations with $c = 0.5$, $u_1$ degenerated into what seemed like random noise whilst $u_2$ became a tall (sometimes with a second smaller peak to the left of the main peak) soliton that was moving in the left direction (negative $\xi$ direction).

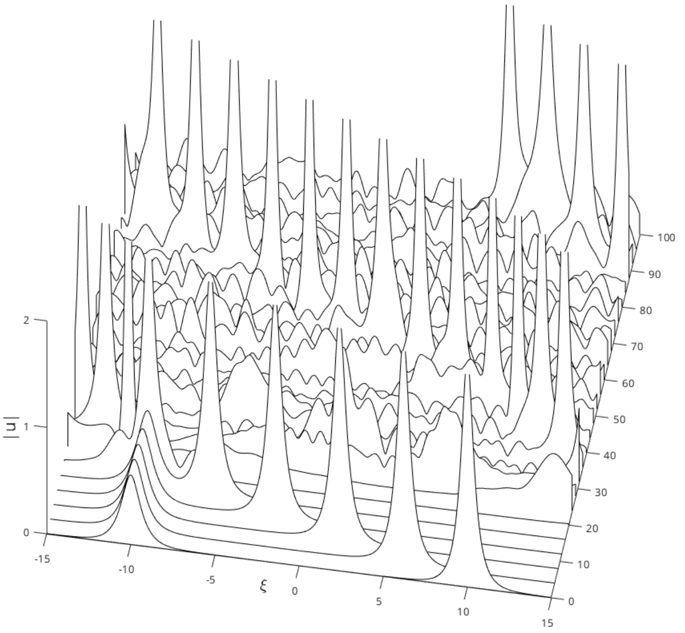

Figure 7: Plot of $u_2$ before, during and after tall and short soliton collision. $c = 0.5$ and $dt = 0.003$ in this collision ($t_{\max} = 100$).

When sine waves of amplitude 0.01 were added to the initial conditions there was no obvious changed to the collision observed. When the amplitude was increased to 0.1 similar behaviour was observed, although the tall soliton was at times wider and shorter than it was without the perturbation. After this the amplitude was increased to 0.5 and no collision occurred.

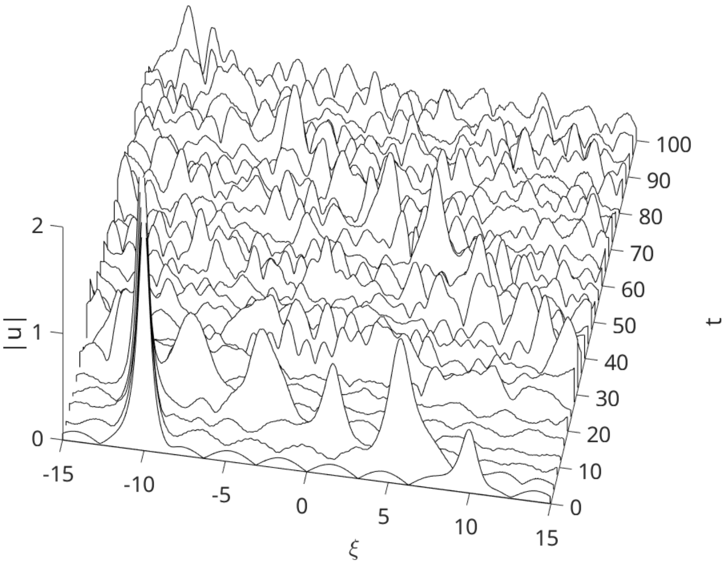

Figure 8: Plot of $u_1$ before, during and after tall and short soliton collision when $u_1$ and $u_2$ have both had $0.1 \sin \xi$ added to their initial conditions. $c = 0.5$ and $dt = 0.003$ in this collision ($t_{\max} = 100$).

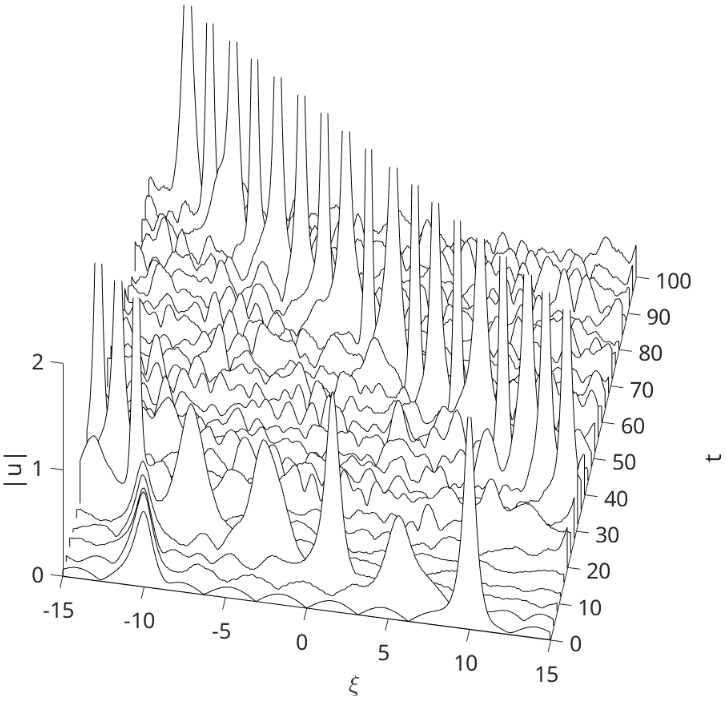

Figure 9: Plot of $u_2$ before, during and after tall and short soliton collision when $u_1$ and $u_2$ have both had $0.1 \sin \xi$ added to their initial conditions. $c = 0.5$ and $dt = 0.003$ in this collision ($t_{\max} = 100$).

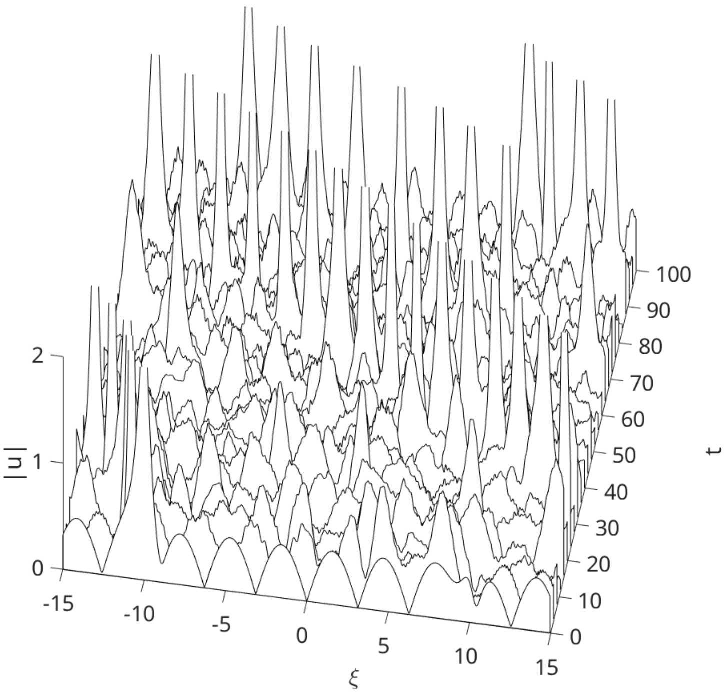

Figure 10: Plot of $u_1$ before, during and after tall and short soliton collision when $u_1$ and $u_2$ have both had $0.5 \sin \xi$ added to their initial conditions. $c = 0.5$ and $dt = 0.003$ in this collision ($t_{\max} = 100$).

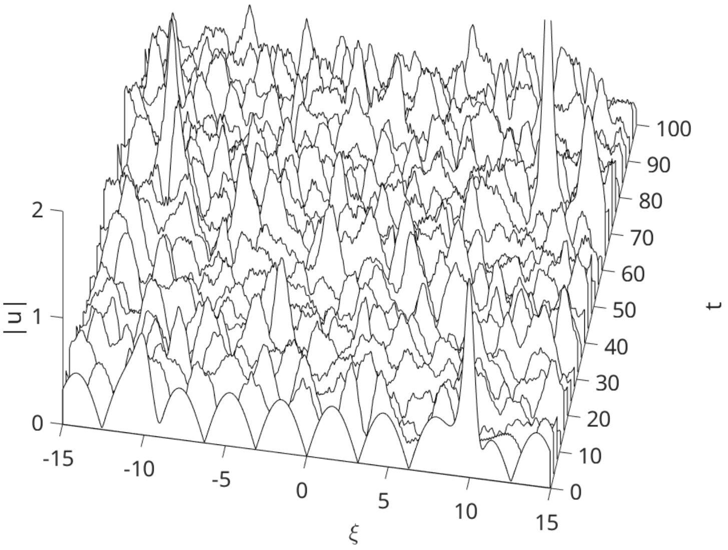

Figure 11: Plot of $u_2$ before, during and after tall and short soliton collision when $u_1$ and $u_2$ have both had $0.5 \sin \xi$ added to their initial conditions. $c = 0.5$ and $dt = 0.003$ in this collision ($t_{\max} = 100$).

Similar patterns were noticed when $c = 0.8$ was used. This includes when perturbations were added to the initial conditions.

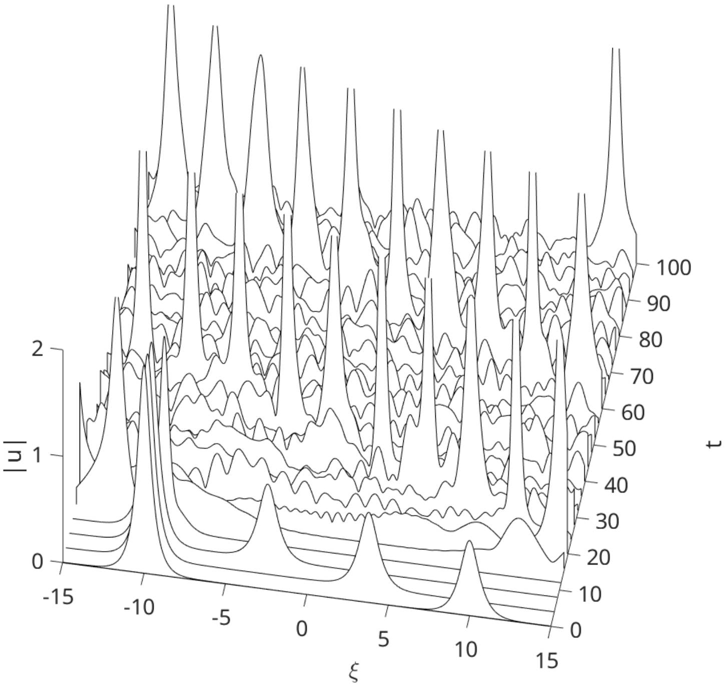

Figure 12: Plot of $u_1$ before, during and after tall and short soliton collision. $c = 0.8$ and $dt = 0.003$ in this collision ($t_{\max} = 100$).

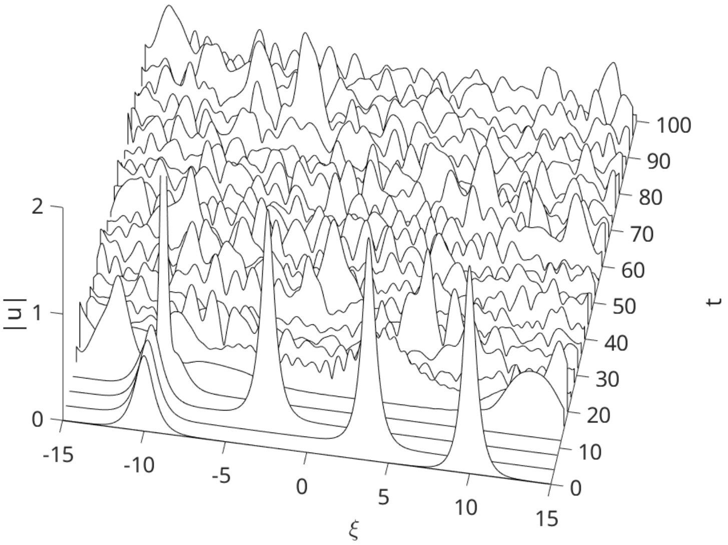

Figure 13: Plot of $u_2$ before, during and after tall and short soliton collision. $c = 0.8$ and $dt = 0.003$ in this collision ($t_{\max} = 100$).

## Discussion and conclusion

This hybrid method of using Fourier spectral methods to approximate spatial derivatives combined with the Runge-Kutta fourth-order method to numerically integrate the problem on time proved effective and useful in solving the coupled NFSEs. It was also useful in modelling the behaviour of Kerr solitons. One issue in this report was that it was sometimes unclear whether what was seen in the graphs was the result of numerical errors or the actual behaviour of the solution. Consequently, future studies should probably try using an adaptive method of time integration such as the Runge-Kutta-Fehlberg method with a set error tolerance. Alternatively, a non-adaptive scheme could be used with multiple different values of $dt$ tried. Multiple different values of $dt$ were not tried in this research due to how slowly the scripts used executed and using multiple different time increments would likely exacerbate this problem. To fix this issue future research could use programs written in higher-performance programming languages like C++, Fortran or Julia.

## Acknowledgements

Dmitry Strunin provided guidance for the project, provided the data files required for it as well as the code to import them and proofed this report. Program 2 of Yang (2010) served as the template of the code used.

## References

R. Driben and B. A. Malomed. Stability of solitons in PT-symmetric couplers. *Optics Letters*, 36(22):4323, Nov. 2011. ISSN 0146-9592, 1539-4794. doi: 10.1364/OL.36.004323.

P. Li, B. A. Malomed, and D. Mihalache. Symmetry breaking of spatial Kerr solitons in fractional dimension. *Chaos, Solitons & Fractals*, 132:109602, Mar. 2020. ISSN 0960-0779. doi: 10.1016/j.chaos.2020.109602.

J. Yang. *Nonlinear Waves in Integrable and Non-integrable Systems.* SIAM, Dec. 2010. ISBN 978-0-89871-705-1.